arXiv:1412.4788v1 [cond-mat.quant-gas] 15 Dec 2014

Photonic Architectures for Equilibrium High-Temperature Bose-Einstein Condensation in Dichalcogenide Monolayers

Jian-Hua Jiang[1,*] and Sajeev John[1]

[1] *Department of Physics, University of Toronto, Toronto, Ontario, M5S 1A7 Canada*

(Dated: December 17, 2014)

* Correspondence to jianhua.jiang.phys@gmail.com

Semiconductor-microcavity polaritons are composite quasiparticles of excitons and photons, emerging in the strong coupling regime. As quantum superpositions of matter and light, polaritons have much stronger interparticle interactions compared with photons, enabling rapid equilibration and Bose-Einstein condensation (BEC). Current realizations based on 1D photonic structures, such as Fabry-Pérot microcavities, have limited light-trapping ability resulting in picosecond polariton lifetime. We demonstrate, theoretically, above-room-temperature (up to 590 K) BEC of long-lived polaritons in $MoSe_2$ monolayers sandwiched by simple TiO_2 based 3D photonic band gap (PBG) materials. The 3D PBG induces very strong coupling of 40 meV (Rabi splitting of 62 meV) for as few as three dichalcogenide monolayers. Strong light-trapping in the 3D PBG enables the long-lived polariton superfluid to be robust against fabrication-induced disorder and exciton line-broadening.

Semiconductor microcavities with engineered photonic states are a valuable platform to observe fundamental and emergent quantum electrodynamic phenomena[1]. Polaritons are formed as a quantum superposition of semiconductor-excitons and microcavity-photons when the exciton-photon interaction is much larger than their decay rates. The ability to tailor the photonic modes, light-matter interaction and polariton lifetime in semiconductor microcavities enables versatile control of polaritons and opens the possibility of novel quantum effects such as Bose-Einstein condensation (BEC) at elevated temperatures[2–6]. Picosecond time-scale quasiequilibrium room-temperature polariton BEC has been claimed in ZnO[7, 8], GaN[9–11], and polymers[12] in Fabry-Pérot microcavities. This is possible when the thermalization time is even shorter than the polariton lifetime. However, for both scientific studies and applications, it is more favorable to achieve room-temperature polariton BEC with polariton lifetimes on the scale of 100 ps - 1 ns. Realization of long-lived, room-temperature, equilibrium polariton BEC remains an important target for fundamental research and practical application[13].

In this article, we demonstrate theoretically a route to simultaneously achieve very strong exciton-photon coupling and long polariton lifetime using a simple TiO_2 based photonic band gap (PBG)[14, 15] material sandwiching a planar quantum-well slab containing as few as three monolayers of the transition-metal dichalcogenide $MoSe_2$[5]. This architecture provides a realistic, technologically accessible route toward equilibrium polariton BEC above

room temperature. In contrast, the corresponding Fabry-Pérot microcavity has picosecond polariton lifetime due to radiative recombination into unwanted leaky (air) modes that are degenerate with the microcavity mode. These leaky modes couple strongly to any finite area polariton condensate in the quantum-well region. They are eliminated by replacing the 1D periodic structure with a 3D PBG material. Recently WSe_2 and MoS_2 monolayers in 2D photonic crystals have been experimentally realized[17, 18]. However, a complete 3D PBG is absent in those cavities and radiative decay of polaritons is not suppressed effectively. Another realization of a MoS_2 monolayer in a Fabry-Pérot microcavity[19] reveals exciton-photon coupling of 31.5 meV but very rapid (sub-picosecond) polariton decay and significant line-broadening of 38.5 meV.

In a $MoSe_2$ monolayer the exciton binding energy is as large as 0.55 eV and the exciton Bohr radius is as small as 1.2 nm[2, 5]. Theoretical calculation[5] predicts that 6% of incident light is absorbed during transmission through a $MoSe_2$ layer[5], indicating very strong light-matter interaction. As we show, this enables high-temperature BEC with only three quantum-well monolayers of $MoSe_2$. Previous considerations of high-temperature, equilibrium BEC have involved on the order of 100 quantum-wells[14]. Another special property of $MoSe_2$ is that due to correlation between wave-vector valley and spin polarizations at the electronic band edge of $MoSe_2$, left- and right-circularly polarized light are coupled to different exciton spin and valley states[1]. In other words, optical, valley, and spin polarizations are correlated with each other. Information encoded in the spin and valley channels of the condensate can be uncovered by measuring the polarization of emitted light. This may provide a new degree of freedom to store and manipulate coherent quantum information in the predicted polariton condensate[23–25].

OPTICAL MICROCAVITY ARCHITECTURES

A fundamental challenge to the realization of above-room-temperature BEC is the accurate fabrication of complex photonic nanostructures. Almost all previous experimental studies have focused on 1D dielectric multi-layers which provide strong exciton-photon coupling at the expense of concomitant strong coupling to low-quality-factor leaky modes that render picosecond time-scale polariton lifetimes. 3D PBG materials enable very strong coupling without the occurrence of leaky modes. However, structures made of CdTe[14] require

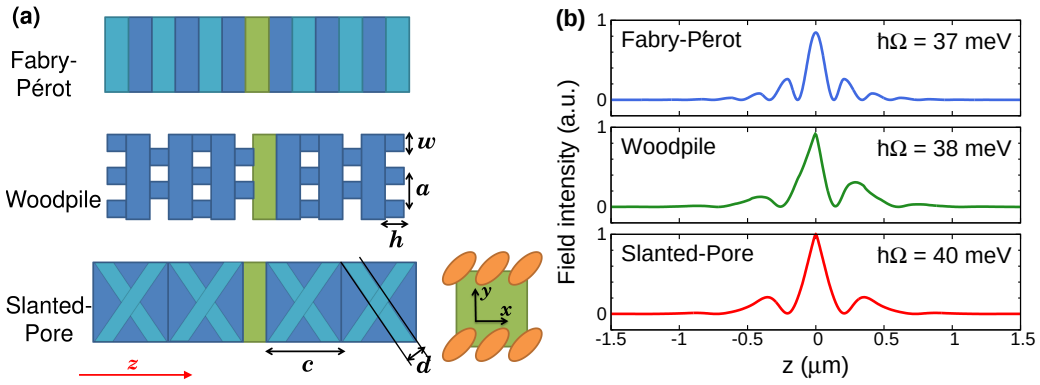

FIG. 1. **Strong coupling in microcavities** (a) Schematics of the FP, woodpile PC and SP PC microcavities. Green regions in the middle represent the active layer containing 3 $MoSe_2$ monolayers embedded in TiO_2 for the PC cavities and SiO_2 for the FP cavity. For the FP cavity, the dark-blue regions are TiO_2 while the light-blue regions are SiO_2. For woodpile PC cavity the white regions denote the air regions while the blue regions are TiO_2. For SP PC cavity the light-blue regions denote slanted air pores while the dark-blue regions are TiO_2. Top view of the active layer for the SP structure depicts breaking of x-y symmetry due to adjacent air pores, leading to the lifting of polariton ground state degeneracy. (b) The distributions of the averaged in-plane photonic field intensity, $S_{u.c}^{-1}\int_{u.c.} d\vec{\rho}(|\mathcal{E}_{\vec{q}}^{x}|^2+|\mathcal{E}_{\vec{q}}^{y}|^2)$ at $\vec{Q}=(0,\frac{\pi}{a},0)$, along z direction for the woodpile PC and SP PC cavities, and that at $\vec{Q}=0$ for the FP cavity.

a very large number of embedded quantum wells in the active region to provide sufficiently strong coupling to approach room temperature BEC. Here, we propose a simple route to above-room-temperature BEC using TiO_2-based photonic crystal architectures. As a reference, we provide comparison with a corresponding TiO_2-SiO_2 1D multi-layer photonic cavity.

In Fig. 1 we depict the Fabry-Pérot (FP), woodpile photonic crystal (PC) and slanted-pore (SP) PC microcavities, as well as their cavity-mode field intensities along the growth z-direction. There are 3 $MoSe_2$ monolayers in the middle of each microcavity separated by 7 nm TiO_2 layers (SiO_2 for the FP). Inter-layer Coulomb correlation energy is suppressed due to the large static dielectric constant (~ 100) of TiO_2 at room temperature[26]. The Coulomb interaction energy for two electrons (holes) separated by $\geq$7 nm with such high dielectric constant is $\lesssim$2 meV, which is much smaller than other energy scales such as the exciton-photon coupling $\hbar\Omega = 40$ meV. Consequently, we treat excitons in each monolayer

as independent. The structures of 3 microcavities are illustrated in Fig. 1a. In the woodpile PC, the height of each rod is $h = 0.3a$ and the width is $w = 0.25a$ where $a \simeq 380$ nm is the periodicity in the x-y plane (see Fig. 1a). The SP PC cavity is a SP_2 structure of the $\mathbf{S}/[1,1] \oplus [-1,-1]^{(0.5,0)}$ family[27] with the periodicity along the z direction of $c = 1.4a$ where $a \simeq 370$ nm is the in-plane lattice constant. The diameter of each cylindrical air pore is $d = 0.69a$. For both types of PC microcavity, the thickness of the slab is $0.05a$. The SiO_2-TiO_2 FP cavity has two Bragg mirrors with periodicity of $a \simeq 210$ nm and a half-wave SiO_2 slab of thickness $\simeq 270$ nm in the middle, such that the lowest band edge cavity mode is close to the exciton recombination energy of 1.55 eV.

Sandwiched PC–quantum-well–PC structures[18, 19] are fabricated in a layer-by-layer process[12, 13]. The PCs and the quantum-well structure are fabricated independently, the quantum-well structure is then fused onto the lower PC and finally the upper PC is fused onto the quantum-well structure[12, 13]. Corresponding technologies for TiO_2 PC growth have become mature in the last decade[32–36]. In addition, high quality $MoSe_2$ thin films can be grown by molecular beam epitaxy[5] and chemical vapor deposition[17].

The 3D PBG's in the woodpile and the SP PC's are $\delta\omega/\omega_c = 8.7\%$ and 14%, respectively ($\delta\omega$ and ω_c are the bandwidth and the central frequency of the PBG, respectively). Photonic band structures near the 3D-PBG for the woodpile and SP PC cavities reveal several confined 2D guided bands in the PBG, among which only the lowest one (depicted in Fig. 2) is relevant for polariton BEC[14].

STRONG EXCITON-PHOTON COUPLING

The Hamiltonian of the coupled exciton-photon system can be written as[14]

$$H = \sum_{\vec{q}} \Big[\sum_{l,I_z} E_X(\vec{q}) b^\dagger_{l,I_z,\vec{q}} b_{l,I_z,\vec{q}} + \hbar\omega_{\vec{q}} a^\dagger_{\vec{q}} a_{\vec{q}} \Big] + H_I, \tag{1a}$$

$$H_I = \sum_{l,I_z,\vec{q}} i\hbar\overline{\Omega}_{l,I_z,\vec{q}} (b^\dagger_{l,I_z,\vec{q}} a_{\vec{q}} - a^\dagger_{\vec{q}} b_{l,I_z,\vec{q}}), \tag{1b}$$

where $b^\dagger_{l,I_z,\vec{q}}$ creates an exciton in the l-th monolayer with total angular momentum $\hbar I_z = \pm\hbar$ along z direction. The energy of the $1s$-exciton is $E_X(\vec{q}) = E_{X0} + \frac{\hbar^2 q^2}{2m_X}$ where $E_{X0} = 1.55$ eV and m_X are exciton emission energy and effective mass, respectively. In this optical transition from valence to conduction band, the electron spin is preserved but its orbital

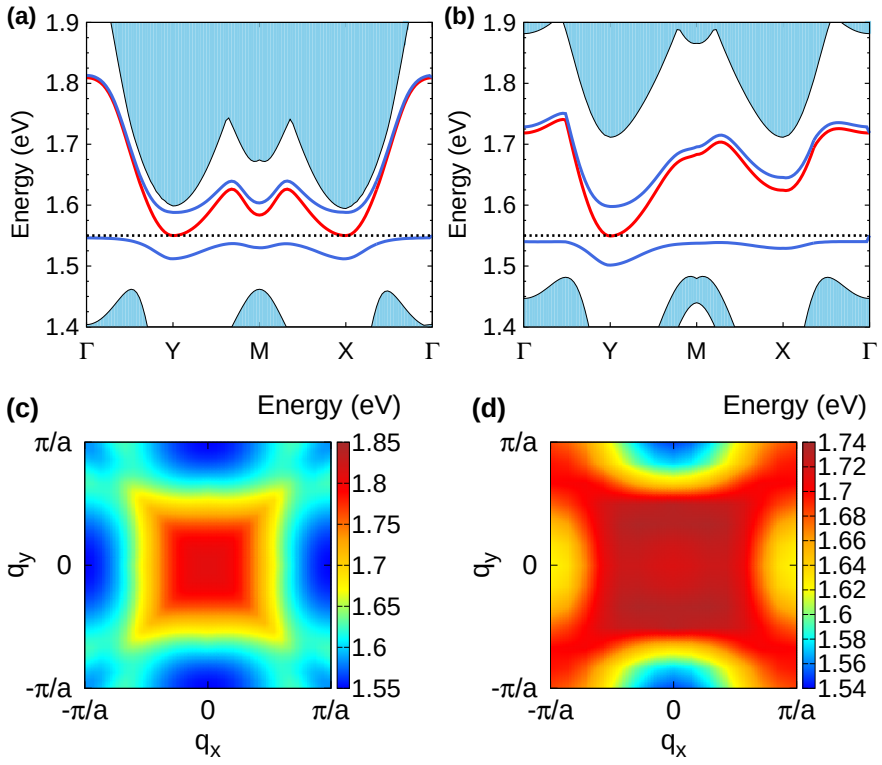

FIG. 2. **Photonic and polaritonic band structures**. Spectra of photon, exciton, and polariton for (a) woodpile and (b) SP PC microcavities. Light-blue regions are 3D photonic bands. The red curves are the lowest 2D planar guided modes, the dotted curves denote the exciton recombination energy, and the blue curves represent the upper and lower polariton branches. The lowest band edges of the 2D guided (cavity) modes are in resonance with the exciton recombination energy, 1.55 eV. This is realized when $a = 380$ nm for the woodpile and $a = 370$ nm for the SP PC. Spectra of the lowest 2D planar guided photonic band in 2D wave-vector space for woodpile (c) and SP (d) PC microcavities. The polariton ground state is doubly degenerate for the woodpile but nondegenerate for the SP microcavity.

angular momentum changes by $\hbar$. $a^\dagger_{\vec{q}}$ creates a photon with wave-vector $\vec{q}$ and frequency $\hbar\omega_{\vec{q}}$ in the lowest guided 2D photonic band. The exciton-photon coupling is

$$\hbar\overline{\Omega}_{l,I_z,\vec{q}} = \frac{d_{cv}|\phi(0)|\sqrt{\hbar\omega_{\vec{q}}}}{\sqrt{2\varepsilon_0}}\sqrt{\int_{u.c.}\frac{d\vec{\rho}}{S_{u.c.}}|u_{I_z,\vec{q}}(\vec{\rho},z_l)|^2}, \tag{2}$$

where $d_{cv} = 3.6\times10^{-29}$ Cm (Supplementary Information) is the absolute value of the interband dipole matrix element, $\phi(0)$ is the exciton wavefunction of the $1s$-excitonic state at zero electron-hole distance, ϵ_0 is the vacuum permittivity, $S_{u.c.} = a^2$ is the area of the

unit cell of PC in the x-y plane, z_l is the z coordinate of the l-th $MoSe_2$ monolayer plane. $u_{I_z,\vec{q}} = \vec{\mathbf{e}}_{I_z} \cdot \vec{u}_{\vec{q}}$ where $\vec{\mathbf{e}}_{I_z} = \frac{1}{\sqrt{2}}(1, -iI_z, 0)$ is the polarization vector of the exciton state with $I_z = \pm 1$ and $\vec{u}_{\vec{q}}(\vec{r})$ is the periodic part of the photonic electric field $\vec{\mathcal{E}}_{\vec{q}}(\vec{r}) = \sqrt{\frac{\hbar\omega_{\vec{q}}}{2\varepsilon_0 S}}\vec{u}_{\vec{q}}(\vec{r})e^{i\vec{q}\cdot\vec{\rho}}$. Here S is the area of the system, $\vec{r} = (\vec{\rho}, z)$ with $\vec{\rho} = (x, y)$ and $S_{u.c.}^{-1}\int_{u.c.} d\vec{\rho}dz\epsilon(\vec{r})|\vec{u}_{\vec{q}}(\vec{r})|^2 = 1$. The special electronic band structure (see Fig. 3a) leads to optical selection rules for the lowest excitonic transitions: the σ_+ photon excites only spin-up $J_z = \frac{3}{2}\hbar$ hole and spin-down $J_z = -\frac{1}{2}\hbar$ electron in the $\mathbf{K}$ valley, while σ_- photon excites only spin-down $J_z = -\frac{3}{2}\hbar$ hole and spin-up $J_z = \frac{1}{2}\hbar$ electron in the $-\mathbf{K}$ valley[1, 38, 39]. Here J_z is the total angular momentum along z direction.

The resulting dispersion of the lower polariton branch is

$$E_{lp}(\vec{q}) = \frac{E_X(\vec{q}) + \hbar\omega_{\vec{q}}}{2} - \left[\left(\frac{E_X(\vec{q}) - \hbar\omega_{\vec{q}}}{2}\right)^2 + \hbar^2\Omega_{\vec{q}}^2\right]^{1/2}. \quad (3)$$

Here the collective exciton-photon coupling[14] is given by $\Omega_{\vec{q}}^2 = \sum_{l,I_z}|\overline{\Omega}_{l,I_z,\vec{q}}|^2$. Strong light trapping leads to exciton-photon interaction as large as 40 meV and 38 meV in the SP PC and woodpile PC microcavities, respectively.

ABOVE ROOM TEMPERATURE POLARITON BEC

The polariton BEC transition temperature, T_c, is calculated by the criterion[40] $N_0/N_{tot} = 10\%$ where N_0 and N_{tot} are the population on the ground state and the total polariton number respectively[40]. We consider a quantum box trap for polaritons with box area defined by the finite area of embedded $MoSe_2$ thin films. As shown below, the trap size, characterized by the side length D of the square box, does not alter the transition temperature considerably over a range from a few microns to one centimeter. The quantum box confinement leads to quantization of wave-vector and energy. At thermal equilibrium, $N_0 = [e^{(E_0-\mu)/(k_BT)} - 1]^{-1}$, $N_{tot} = \sum_j [e^{(E_j-\mu)/(k_BT)} - 1]^{-1}$, where E_0 is the ground state energy, j runs over all discrete energy levels, and μ is the chemical potential. As shown previously[14], T_c is essentially defined by the polariton dispersion depth, $V_{lp} \equiv \Delta/2 + \sqrt{(\Delta/2)^2 + \hbar^2\Omega^2}$, where $\Delta = E_{X0} - \hbar\omega_0$ is the exciton-photon detuning and $\hbar\Omega \equiv \hbar\Omega_{\vec{Q}^{(\nu)}}$ is the exciton-photon coupling at photonic band edge. As k_BT approaches V_{lp}, the population on exciton-like states with very large effective mass becomes significant[14]. The pure exciton BEC transition temperature is calculated to be less than 4 K for density less than $(10a_B)^{-2}$ and trap size D of 1 micron in a

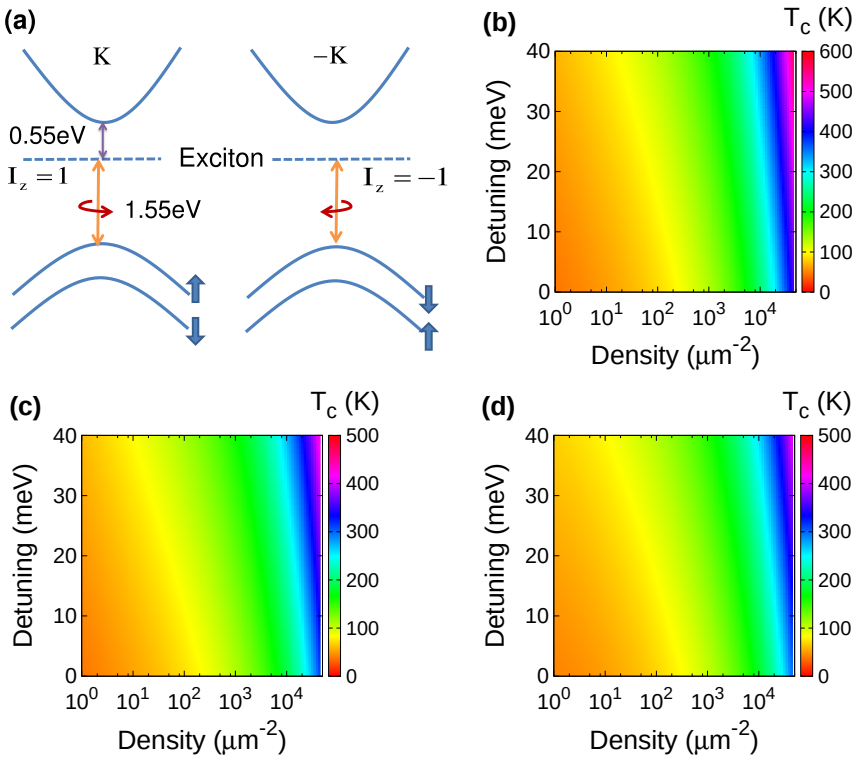

FIG. 3. **Optical selection rules and polariton BEC transition temperatures in $MoSe_2$ cavities** (a) Electronic band structure and optical selection rules for $MoSe_2$. The spin-degeneracy in the valence band is lifted by spin-orbit interaction. For an excitonic optical transition, the σ_+ photon (angular momentum parallel to its wave-vector) is coupled to an exciton in the **K** valley consisting of a spin-up $J_z = \frac{3}{2}\hbar$ hole and a spin-down $J_z = -\frac{1}{2}\hbar$ electron. The σ_- photon is coupled to an exciton in the $-\mathbf{K}$ valley consisting of a spin-down $J_z = -\frac{3}{2}\hbar$ hole and a spin-up $J_z = \frac{1}{2}\hbar$ electron. Polariton BEC transition temperature T_c vs. detuning Δ and polariton density for (b) SP PC, (c) woodpile PC and (d) FP microcavities. The side length of the square-shaped exciton-trap is $D = 5$ μm.

$MoSe_2$ monolayer. On the other hand for positive detuning $\Delta = 30$ meV and $\hbar\Omega = 40$ meV, the dispersion depth is 58 meV. This can support polariton BEC up to $V_{lp}/k_B \simeq 600$ K.

Figs. 3(b)-(d) give the polariton BEC transition temperatures for different detuning Δ and polariton densities for the SP PC, woodpile PC, and FP cavities. We assume that the exciton gas is initially created by incoherent pumping that (after thermal relaxation) equally populates all degenerate dispersion minima ($\vec{Q}$-points) in the photonic band structure. As seen in Fig. 2, the woodpile PC has a doubly degenerate polariton minimum whereas the

polariton ground state is nondegenerate for the SP PC. The trap size is $D = 5$ μm. The T_c is enhanced with increasing detuning as the polariton dispersion depth increases. The highest T_c is reached at the largest detuning $\Delta = 40$ meV which is 590 K, 450 K, and 430 K for the SP PC, woodpile PC and FP cavities, respectively. The BEC transition temperature T_c is highest in the SP PC cavity since it contains a nondegenerate polariton ground state. This is provided by the placement of the active layer at a plane that breaks the x-y symmetry of the criss-crossing pores above and below (see Fig. 1a). In contrast, there are two degenerate polariton minima in the woodpile that reduces effective polariton density for BEC by a factor of two. In the case of the FP cavity, the polariton density available for BEC is divided by the two degenerate optical polarization states at $\vec{Q} = 0$. We do not consider larger detuning because a too large Δ will reduce the exciton fraction of polariton as well as the polariton-phonon and polariton-polartion scattering, which leads to much longer equilibration time.

The polariton BEC transition temperatures at $\Delta = 30$ meV for different trap sizes D and polariton densities for each cavity are shown in Fig. 4. The trap size dependence is prominent for low polariton densities, but very weak for high polariton densities[14]. At low densities, $k_B T_c \ll V_{lp}$ and polariton equilibrium is governed by the low-lying excited states of very small effective mass particles in the box trap that are very sensitive to D. At high polariton densities, $k_B T_c \lesssim V_{lp}$ and a significant fraction of polaritons acquire the bare exciton mass for which the level spacing is less sensitive to D. Eventually T_c tends to zero for very large trap size D (when the low-lying excited states are extremely close to the ground state) according to the Mermin-Wagner theorem[8]. In all these calculations the largest polariton density, 5×10^4 μm^{-2}, corresponds to an exciton density in each $MoSe_2$ monolayer less than $(11a_B)^{-2}$, well below the exciton saturation density of $(5a_B)^{-2}$[42].

Fabrication induced disorder and exciton line broadening tend to degrade high-temperature polariton BEC. In a PBG material, light in the cavity mode is well-protected from scattering into unwanted modes. Consequently, the role of disorder is primarily to shift the cavity resonance frequency. For photonic (dielectric) disorder, our calculation indicates that in the woodpile and SP PC cavities, photonic structure deviations less than 6 nm in the active slab layer, less than 12 nm in the logs close to the active slab layer, or less than 20 nm in the logs two periods away, do not affect the band edge of the lowest planar guided mode by more than 2%. This fluctuation is equivalent to alteration of the detuning by ± 30 meV,

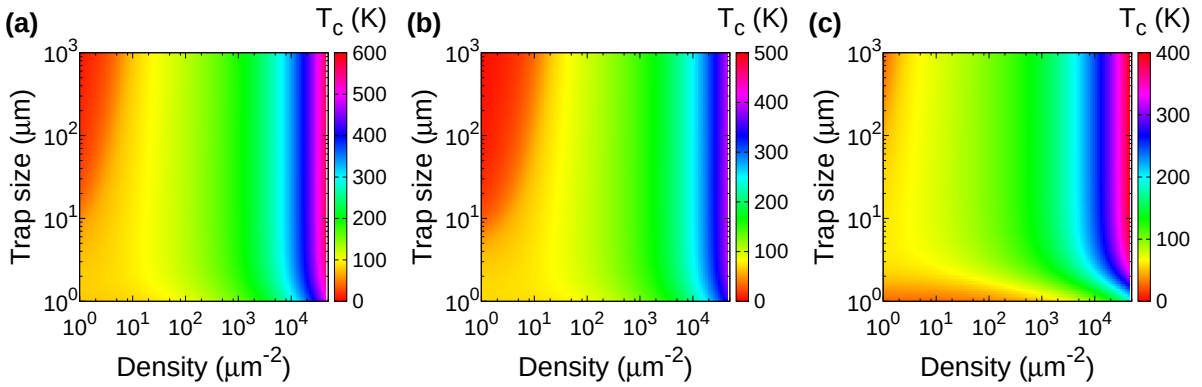

FIG. 4. **High-temperature polariton BEC** Polariton BEC transition temperature T_c vs. trap size and polariton density for (a) SP PC, (b) woodpile PC, (c) FP microcavities. Detuning is $\Delta = 40$ meV, corresponding to $\lambda = 820$ nm for the FP cavity, $a = 390$ nm for woodpile PC cavity, and $a = 380$ nm for SP PC cavity.

which can reduce the T_c to 360 K (480 K) if the detuning decreases to 10 meV for the woodpile (SP) PC cavity. Polariton BEC is also found to be robust to exciton homogeneous and inhomogeneous broadening although the Rabi-splitting and polariton dispersion depth are slightly reduced (e.g., Rabi splitting in SP cavity is reduced from 80 meV to 62 meV) (see Supplementary Information).

In contrast there is no 3D PBG for the FP cavity and light-trapping is not robust to disorder. Excitons in the FP with wave-vector $q \gtrsim 0.3q_0$ with $q_0 = E_{X0}/(\hbar c)$ are strongly coupled to leaky (air) modes, leading to rapid radiative decay[43]. This decay into leaky modes is not alleviated by increasing the quality of the FP cavity mode and is exacerbated by imperfect fabrication accuracy. In real FP cavities, dielectric disorder scatters polaritons with wave-vector $q \sim 0$ into leaky modes with the same energy. Such scattering significantly limits the quality factor of the (nonleaky) cavity mode ($\sim 10^3$). The overall polariton lifetime due to radiative decay is very short ($\lesssim 1$ ps) in SiO_2/TiO_2 multilayers[9] and in other[8] FP cavities. The resulting sub-picosecond polariton lifetime (see also calculation in the Supplementary Information) is still comparable with the thermalization time, although calculations have shown that phonon scattering is very efficient (about 0.1 ps scattering time) in $MoSe_2$ at room temperature[45]. In contrast, PC cavities protected by a 3D PBG enable light-trapping in all directions, leading to polaritons with lifetime limited only by nonradiative decay (see Supplementary Information). This nonradiative decay is further suppressed

by our detuning ($\Delta > 0$) that renders our polariton more photon-like than exciton-like. The quantum coherence of polaritons in the cavity can be probed and manipulated using light propagating through engineered waveguide channels in the 3D PBG cladding[13, 46].

In the absence of any microcavity, optically excited valley polarization of excitons can last only about 9 ps in $MoSe_2$ at room temperature[6]. In high-quality PC microcavities strong light trapping over all directions can enhance polariton lifetime beyond 130 ps (the exciton lifetime in $MoSe_2$ monolayer without any cavity at room temperature)[6]. When the polaritons form a BEC, optical, valley, and spin polarization coherences maintained on such long time-scales may be useful for quantum information processing based on manipulation of the spin and valley degrees of freedom[24, 25].

CONCLUSIONS

We have theoretically demonstrated photonic crystal architectures based on TiO_2 with very strong light-matter interaction and long polariton lifetime for above-room-temperature, equilibrium exciton-polariton BEC. The 3D photonic band gap robustly supports strongly confined guided modes in a slab cavity containing three separated excitonic $MoSe_2$ monolayers. Unlike 1D periodic Fabry-Pérot structures that suffer from substantial radiative decay through directions other than the stacking direction, the 3D PBG structures suppress radiative decay in all directions enabling equilibration and long-time polariton coherence. An important feature of the slanted pore PC architecture is that it provides a non-degenerate lower polariton dispersion minimum, without recourse to a symmetry-breaking external field[23]. This enables a remarkable equilibrium high-temperature Bose-Einstein condensate, above 500 K, with only three quantum well layers. Both TiO_2 based photonic crystals and $MoSe_2$ thin films have been fabricated with mature technologies providing a very accessible route to high-temperature BEC. This BEC is robust to disorder, fabrication imperfections, exciton homogeneous and inhomogeneous line-broadening. The unique coupling among the optical, valley, and spin degrees of freedom in $MoSe_2$ provides a condensate with novel internal symmetries that can be manipulated by external fields. Polariton BEC with long-lived optical, valley, and spin coherence persisting above room-temperature offers new opportunities for macroscopic quantum physics.

METHODS

The photonic band structures and electric field distributions for PC microcavities are calculated using the plane wave expansion method, while those for the FP microcavity are calculated using the transfer matrix method. The refractive indices of TiO_2 and SiO_2 are 2.7 and 1.5, respectively[48]. In $MoSe_2$ the effective mass for conduction band electron and valence band hole are, $m_e = 0.7m_0$ and $m_h = 0.55m_0$, respectively[4]. The effective mass of exciton is $m_X = m_e + m_h$. The exciton Bohr radius a_B and interband band dipole matrix element d_{cv} are obtained from existing studies on electronic band structure in $MoSe_2$ and excitonic optical absorption[1, 5] (see Supplementary Information). The calculation of T_c involves summation over numerous polariton states which is broken into two parts: the summation over the first 1600 states and the integration over other higher states. Polariton energy in a square (hard-wall) quantum box is calculated according to wave-vector quantization.

[1] Yamamoto, Y., Tassone, T. & Cao, H. *Semiconductor cavity quantum electrodynamics*. (Springer, Berlin, 2000).

[2] Deng, H., Weihs, G., Santori, C., Bloch, J., & Yamamoto, Y. Condensation of semiconductor microcavity exciton polaritons. *Science* **298**, 199-202 (2002).

[3] Kasprzak, J. *et al.* Bose-Einstein condensation of exciton polaritons. *Nature* **443**, 409-414 (2006).

[4] Balili, R., Hartwell, V., Snoke, D., Pfeiffer, L., West, K. Bose-Einstein condensation of microcavity polaritons in a trap. *Science* **316**, 1007-1010 (2007).

[5] Kasprzak, J., Solnyshkov, D. D., André, R., Dang, L. S. & Malpuech, G. Formation of an exciton polariton condensate: thermodynamic versus kinetic regimes. *Phys. Rev. Lett.* **101**, 146404 (2008).

[6] Deng, H., Haug, H. & Yamamoto, Y. Exciton-polariton Bose-Einstein condensation. *Rev. Mod. Phys.* **82**, 1489-1537 (2010).

[7] Lai, Y.-Y., Lan, Y.-P. & Lu, T.-C. Strong light-matter interaction in ZnO microcavities. *Light Sci. Appl.* **2**, e76 (2013).

[8] Li, F. *et al.* From excitonic to photonic polariton condensate in a ZnO-based microcavity. *Phys. Rev. Lett.* **110**, 196406 (2013).

[9] Christopoulos, S. *et al.* Room-temperature polariton lasing in semiconductor microcavities. *Phys. Rev. Lett.* **98**, 126405 (2007).

[10] Christmann, G., Butté, R., Feltin, E., Carlin, J.-F. & Grandjean, N. Room temperature polariton lasing in a GaN/AlGaN multiple quantum well microcavity. *Appl. Phys. Lett.* **93**, 051102 (2008).

[11] Levrat, J. *et al.* Condensation phase diagram of cavity polaritons in GaN-based microcavities: experiment and theory. *Phys. Rev. B* **81**, 125305 (2010).

[12] Plumhof, J. D., Stöferle, T., Mai, L., Scherf, U. & Mahrt, R. F. Room-temperature Bose-Einstein condensation of cavity exciton-polaritons in a polymer. *Nat. Mater.* **13**, 247-252 (2014).

[13] Snoke, D. Microcavity polaritons: a new type of light switch. *Nat. Nanotechnol.* **8**, 393-395 (2013).

[14] John, S. Strong localization of photons in certain disordered dielectric superlattices. *Phys. Rev. Lett.* **58**, 2486-2489 (1987).

[15] Yablonovitch, E. Inhibited spontaneous emission in solid-state physics and electronics. *Phys. Rev. Lett.* **58**, 2059-2062 (1987).

[16] Ugeda, M. M. *et al.* Observation of giant bandgap renormalization and excitonic effects in a monolayer transition metal dichalcogenide semiconductor. arXiv:1404.2331, *Nat. Mater.* in press.

[17] Gan, X. *et al.* Controlling the spontaneous emission rate of monolayer MoS_2 in a photonic crystal nanocavity. *Appl. Phys. Lett.* **103**, 181119 (2013).

[18] Wu, S. *et al.* Control of two-dimensional excitonic light emission via photonic crystal. *2D Mater.* **1**, 011001 (2014).

[19] Liu, X. *et al.* Strong light-matter coupling in two-dimensional atomic crystals. *arXiv*:1406.4826

[20] Ross, J. S. *et al.* Electrical control of neutral and charged excitons in a monolayer semiconductor. *Nat. Commun.* **4**, 1474 (2013).

[21] Jiang, J. H. & John, S. Photonic crystal architecture for room temperature equilibrium Bose-Einstein condensation of exciton-polaritons. *Phys. Rev. X* **4**, 031025 (2014).

[22] Xiao, D., Liu, G.-B., Feng, W., Xu, X. & Yao, W. Coupled spin and valley physics in monolayers of MoS_2 and other group-VI dichalcogenides. *Phys. Rev. Lett.* **108**, 196802 (2012).

[23] Schneider, C. *et al.* An electrically pumped polariton laser. *Nature* **497**, 348-352 (2013)

[24] Amo, A. *et al.* Exciton-polariton spin switches. *Nature Photon.* **4**, 361-366 (2010)

[25] Cerna, R. *et al.* Ultrafast tristable spin memory of a coherent polariton gas. *Nat. Commun.* **4**, 2008 (2013).

[26] Parker, R. A. Static dielectric constant of rutile (TiO_2), 1.6-1060 K. *Phys. Rev.* **124**, 1719-1722 (1961).

[27] Toader, O., Berciu, M., & John, S. Photonic band gaps based on tetragonal lattices of slanted pores. *Phys. Rev. Lett.* **90**, 233901 (2003).

[28] John, S. & Yang, S. Electromagnetically induced exciton mobility in a photonic band gap. *Phys. Rev. Lett.* **99**, 046801 (2007).

[29] Yang, S. & John, S. Exciton dressing and capture by a photonic band edge. *Phys. Rev. B* **75**, 235332 (2007).

[30] Ogawa, S., Imada, M., Yoshimoto, S., Okano, M., & Noda, S. Control of light emission by 3D photonic crystals. *Science* **305**, 227-229 (2004)

[31] Noda, S., Fujita, M., & Asano, T. Spontaneous-emission control by photonic crystals and nanocavities. *Nature Photon.* **1**, 449-458 (2007).

[32] Noda, S., Tomoda, K., Yamamoto, N. & Chutinan, A. Full three-dimensional photonic bandgap crystals at near-infrared wavelengths. *Science* **289**, 604-606 (2000).

[33] Nelson, E. *et al.* Epitaxial growth of three-dimensionally architecture optoelectronic devices. *Nat. Mater.* **10**, 676-681 (2011).

[34] King, J. S. *et al.* Infiltration and inversion of holographically defined polymer photonic crystal templates by atomic layer deposition. *Adv. Mater.* **18**, 1561-1565 (2006).

[35] Deubel, M., Wegener, M., Kaso, A. & John, S. Direct laser writing and characterization of "slanted-pore" photonic crystals. *Appl. Phys. Lett.* **85**, 1895-1897 (2004).

[36] Deubel, M. *et al.* Direct laser writing of three-dimensional photonic-crystal templates for telecommunications. *Nat. Mater.* **3**, 444-447 (2004).

[37] Shim, G. W. *et al.* Large-area single-layer $MoSe_2$ and its van der Waals heterostructures. *ACS Nano* **8**, 6655-6662 (2014).

[38] Zeng, H., Dai, J., Yao, W., Xiao, D. & Cui, X. Valley polarization in MoS_2 monolayers by optical pumping. *Nat. Nanotechnol.* **7**, 490-493 (2012).

[39] Mak, K. F., He, K., Shan, J. & Heinz, T. F. Control of valley polarization in monolayer MoS_2 by optical helicity. *Nat. Nanotechnol.* **7**, 494-498 (2012).

[40] Penrose, O. & Onsager, L. Bose-Einstein condensation and liquid helium. *Phys. Rev.* **104**, 576-584 (1956).

[41] Mermin, N. D. & Wagner, H. Absence of Ferromagnetism or antiferromagnetism in one- or two-Dimensional isotropic Heisenberg models. *Phys. Rev. Lett.* **17**, 1133-1136 (1966).

[42] Schmitt-Rink, S., Chemla, D. S. & Miller, D. A. B. Theory of transient excitonic optical nonlinearities in semiconductor quantum-well structures. *Phys. Rev. B* **32**, 6601-6609 (1985).

[43] Savona, V. & Tassone, F. Exact Quantum Calculation of polariton dispersion in semiconductor microcavities. *Solid State Commun.* **95**, 673-678 (1995).

[44] Bhattacharya, P. *et al.* Room temperature electrically injected polariton laser. *Phys. Rev. Lett.* **112**, 236802 (2014).

[45] Jin, Z., Li, X., Mullen, J. T. & Kim, K. W. Intrinsic transport properties of electrons and holes in monolayer transition-metal dichalcogenides. *Phys. Rev. B* **90**, 045422 (2014).

[46] Chutinan, A., John, S. & Toader, O. Diffractionless flow of light in all-optical microchips. *Phys. Rev. Lett.* **90**, 123901 (2003).

[47] Kumar, N., He, J., He, D., Wang, Y. & Zhao, H. Valley and spin dynamics in $MoSe_2$ two-dimensional crystals. *Nanoscale*, **6**, 12690 (2014).

[48] Landmann, M., Rauls, E. & Schmidt, W. G. The Electronic structure and optical response of rutile, anatase and brookite TiO_2. *J. Phys.: Condens. Matter* **24**, 195503 (2012).

[49] Ramasubramaniam, A. Large excitonic effects in monolayers of molybdenum and tungsten dichalcogenides. *Phys. Rev. B* **86**, 115409 (2012).

ACKNOWLEDGMENTS

We thank J. E. Sipe, J.-L. Cheng, and R. A. Muniz for helpful discussions. This work was supported by the Natural Sciences and Engineering Research Council of Canada and the United States Department of Energy through Contract No. DE-FG02-06ER46347.

AUTHOR CONTRIBUTIONS

J.-H.J. performed calculations and analysis. S.J. guided the research.

ADDITIONAL INFORMATION

Competing financial interests: The authors declare no competing financial interests.

SUPPLEMENTARY INFORMATION

GUIDED 2D PHOTONIC BAND EDGE

In the woodpile PC cavity the lowest 2D photonic band has two dispersion minima: the X point $\vec{Q}^{(X)} = (\frac{\pi}{a}, 0, 0)$ and the Y point $\vec{Q}^{(Y)} = (0, \frac{\pi}{a}, 0)$. The dispersion has a C_{4v} symmetry, inherited from the D_{2d} symmetry of the woodpile PC cavity. We consider the situation when the 2D photonic band edge is close to the exciton emission energy (i.e., $a = 380$ nm) where the dispersion of the 2D photonic band near the minima $\nu = X, Y$ is $\hbar\omega_{\vec{q}} = \hbar\omega_0 + \frac{\hbar^2(q_x - Q_x^{(\nu)})^2}{2m_x^{(\nu)}} + \frac{\hbar^2(q_y - Q_y^{(\nu)})^2}{2m_y^{(\nu)}}$. Here, $m_x^{(X)} = m_y^{(Y)} \simeq 2.4 \times 10^{-5} m_0$ and $m_x^{(Y)} = m_y^{(X)} \simeq 7.2 \times 10^{-5} m_0$ where m_0 is the bare electron mass in vacuum. In SP PC cavity the dispersion of the lowest 2D photonic band has the C_{2v} symmetry. There is only one dispersion minimum at the Y point where the effective mass is also anisotropic with $m_x = 5.7 \times 10^{-5} m_0$ and $m_y = 2.1 \times 10^{-5} m_0$ for $a = 370$ nm. The effective mass of photon in the FP cavity is $0.68 \times 10^{-5} m_0$ at exciton-photon resonance.

ELECTRONIC BAND STRUCTURE OF $MoSe_2$

Schematic of electronic band structure of $MoSe_2$ monolayer is shown in Fig. 3a in the main text. Band extrema are located at the $\mathbf{K} = (\frac{4\pi}{3a_s}, 0)$ (a_s is the honeycomb lattice constant of $MoSe_2$) and $-\mathbf{K}$ points[1]. Very large splitting occurs between spin-up and -down states of 180 meV[2] in the valence band due to spin-orbit interaction. Denoting the z-components of total, orbital and spin angular momenta as J_z, L_z and S_z, the valence band maximum at the $\mathbf{K}$ valley gives spin-up $J_z = \frac{3}{2}\hbar$ holes (absence of an electron with $L_z = -\hbar$ and $S_z = -\frac{1}{2}\hbar$ in the valence band). Its time-reversal partner $-\mathbf{K}$ valley gives spin-down $J_z = -\frac{3}{2}\hbar$ holes. This special electronic band structure leads to optical selection rules for the lowest excitonic states (see Fig. 3a in the main text): the σ_+ photon excites only spin-up $J_z = \frac{3}{2}\hbar$ hole and spin-down $(J_z, L_z, S_z) = (-\frac{1}{2}\hbar, 0, -\frac{1}{2}\hbar)$ electron in the $\mathbf{K}$ valley, while σ_- photon excites only spin-down $J_z = -\frac{3}{2}\hbar$ hole and spin-up $(J_z, L_z, S_z) = (\frac{1}{2}\hbar, 0, \frac{1}{2}\hbar)$ electron in the $-\mathbf{K}$ valley[1].

ESTIMATION OF THE EXCITON-PHOTON COUPLING IN $MOSE_2$

From Ref. [3] the imaginary part of the optical susceptibility at the energy of the $1s$-exciton state $E_{X0} = \hbar\omega_{X0}$ is given by

$$\mathrm{Im}[\chi(\omega_{X0})] = \frac{2d_{cv}^2|\phi(0)|^2}{L_c\hbar\delta}, \tag{4}$$

where L_c is the quantum well width and $\hbar\delta$ is the homogeneous broadening of the $1s$-exciton state. From measurements of $\mathrm{Im}[\chi(\omega_{X0})]$ we deduce $d_{cv}|\phi(0)|$.

The absorptance for an isolated two-dimensional system with thickness L_c is

$$\alpha = \frac{\omega L_c \mathrm{Im}[\chi(\omega)]}{n\varepsilon_0 c}, \tag{5}$$

where ω and c are the frequency and speed of light, respectively, and n is the refractive index. From Ref. [4] the in-plane dielectric constant is 4.7 for a monolayer $MoSe_2$. Accordingly, we choose the refractive index $n \simeq 2.2$.

For $MoSe_2$ the absorptance $\alpha \simeq 6\%$[5]. It follows from Eqs. (4) and (5) that

$$d_{cv}|\phi(0)| = \sqrt{\frac{0.06n\varepsilon_0 c\hbar\delta}{2\omega_{X0}}}. \tag{6}$$

From Ref. [5] the homogeneous broadening at room-temperature is about 50 meV. Therefore, $d_{cv}|\phi(0)| \simeq 2.4\times10^{-20}$ C which is 2.4 times as large as that of excitons GaAs quantum-wells of width 3 nm ($\simeq 1.0\times10^{-20}$ C). Using $|\phi(0)| = \sqrt{2/(\pi a_B^2)}$ for the 2D exciton and the Bohr radius $a_B = 1.2$ nm[5], we estimate $d_{cv} = 3.6\times10^{-29}$ Cm. This is also comparable with[1] $d_{cv} = \sqrt{2}a_s te/E_g = 3.4\times10^{-29}$ Cm where $a_s = 3.313$ Å[1] is the honeycomb lattice constant of $MoSe_2$, $t = 0.94$ eV[1] is the effective electron hopping parameter, $e = 1.602\times10^{-19}$ C is the electronic charge and $E_g = 2.1$ eV[5] is the electronic band gap of $MoSe_2$.

ULTRA-SHORT POLARITON RADIATIVE LIFETIME IN FABRY-PÉROT MICROCAVITIES

1D periodic microstructures can provide strong coupling to a single high-quality factor optical mode. However the concomitant strong coupling to degenerate leaky modes severely reduces the polariton radiative lifetime. Here, we simulate polariton radiative decay from a finite-size polariton condensate using an extended dipole at the center of a FP cavity by

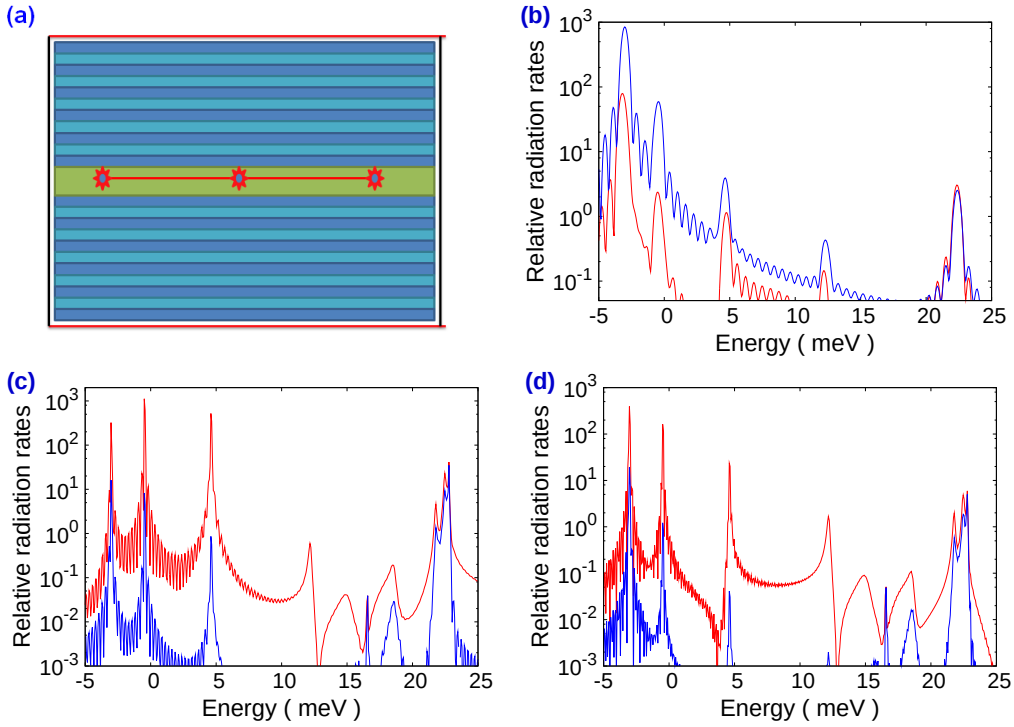

FIG. 5. Supplementary Figure S1. (a) Structure for 2D FDTD calculation of radiation rate in FP cavities. An extended dipole line source with length smaller than the width of the FP cavity is placed in the center (denoted by the line connecting the three star symbols). A Gaussian pulse excites dipole oscillations perpendicular to the paper plane causing outward radiation. The radiation flux is collected at the boundaries surrounding the cavity [denoted by the two red lines (top and bottom) and black lines (left and right)]. The radiation flux is calculated for the FP cavity as well as in the absence of the Bragg mirrors. The ratio of the former over the latter is plotted in (b)-(d). This ratio is resolved into escape through the top and bottom of the cavity (blue curves) and escape through the side directions (red curves). In the simulation, the width of the cavity is 14λ, while the length of the dipole is 12λ or 4λ. The structure is surrounded by an air region of thickness λ followed by perfectly matching layers of thickness 4λ. $\lambda = 0.8$ μm is the length unit and hc/λ is equal to exciton emission energy $E_{X0} = 1.55$ eV. (b)-(d): Dipole radiation rate in FP cavities relative to that in vacuum (red curves) as a function of the detuning of the dipole (exciton) energy from the Fabry-Pérot cavity mode energy. (b) FP cavity with 8 pairs of $\lambda/4$ SiO_2 and TiO_2 layers in the distributed Bragg mirrors above and below the $\lambda/2$ slab. (c) and (d) FP cavities with 15 pairs of $\lambda/4$ layers above and below the slab for different dipole sizes. Simulation is done via 2D FDTD with horizontal dipoles of lengths: (b) and (d) 9.6 μm, (c) 3.2 μm.

finite-difference-time-domain (FDTD). Different dipole sizes are used to represent small and large polariton BEC trap sizes. The radiative decay rate in the FP cavity is compared with that of the same dipole in vacuum (i.e., without the cavity). Experiments[6] suggest that the latter is about 1/(130 ps) in a $MoSe_2$ monolayer at room temperature. 2D FDTD simulations are used to provide a semi-quantitative prognosticator of a realistic 3D structure (see Fig. 5). The radiative decay rate (relative to that in vacuum) for SiO_2-TiO_2 FP cavities with different dipole sizes and numbers of $\lambda/4$ layers are plotted as a function of the detuning of the dipole (exciton) energy from the Fabry-Pérot cavity energy in Fig. 5. The radiative decay is greatly enhanced at some energies while suppressed at other energies all within the exciton homogeneous line-width. The former are the hot-spots for exciton radiative decay leading to very short ($\lesssim 1$ ps) polariton lifetime. In Fig. 5 the zero of energy $hc/\lambda = E_{X0} = 1.55$ eV and all energy scales in the figures are within the 1D photonic stop-gap at normal incidence.

For FP cavities with 8 pairs of $\lambda/4$ SiO_2 and TiO_2 layers (as in Fig. 5a) the cavity mode has a quality factor of 1.2×10^4, implying a cavity photon lifetime of 11 ps. However, excitons can decay radiatively into a broad range of very low quality leaky modes. This radiative decay is most rapid into leaky modes with energy lower than the cavity mode. The 10^3 enhancement of radiation rate leads to sub-picosecond polariton lifetime. With 15 pairs of $\lambda/4$ layers the FP cavity mode has a quality factor as high as 1.8×10^6 implying a cavity photon lifetime of 1500 ps. As before, excitons can radiate through leaky modes (Figs. 5b and 5c) emerging from the sides of the FP. Radiation through leaky modes becomes weaker for the larger dipole size of 12λ than for the smaller dipole size of 4λ. Nevertheless, radiation lifetimes at the hot-spots are on the order of 1 ps. In the limit of an infinitely extended dipole contained in an FP cavity of infinite lateral extent, momentum conservation requires that all radiation is emitted into the cavity mode. However, in this case, BEC is excluded by the Mermin-Wagner theorem[8].

Dielectric disorder in realistic SiO_2-TiO_2 FP's reduces the polariton lifetime even below our calculated time scales[9]. Moreover, at room temperature, excitons with energies away from strongly-coupled leaky modes but within the homogeneous linewidth (50 meV[5]) and phonon energy (43 meV[10]) can be scattered efficiently (within $\lesssim 1$ ps) by phonons[11] to the leaky modes and then radiate rapidly. These effects reduce polariton lifetime to $\lesssim 1$ ps even for FP cavities with 15 pairs of $\lambda/4$ layers and cavity quality factor of 1.8×10^6. The sub-picosecond lifetime of polaritons is still on the same order of magnitude

with the phonon scattering time (about 0.1 ps) in $MoSe_2$ at room temperature[11]. In contrast, in a 3D PBG microcavity architecture with a microcavity embedded in a 3D PBG material[12, 13], all leaky modes can be eliminated leading to very long polariton lifetime, limited only by exciton nonradiative decay. These nonradiative decay channels include Auger recombination arising from exciton-exciton collision and Shockley-Read-Hall recombination arising from electronic defects in the active semiconductor monolayers. Auger recombination is usually very inefficient in moderate to large band gap semiconductors such as $MoSe_2$ for the moderate exciton densities we consider (volume density less than 10^{18} cm^{-3})[7, 14]. Recently high (electronic) quality, large area $MoSe_2$ monolayers were successfully prepared by various methods[15–17], exploiting the significant mechanical, chemical and thermal stability of $MoSe_2$ monolayers[15]. In our architecture, the $MoSe_2$ monolayers are encapsulated by TiO_2 layers above and below, protecting them from defects introduced by wafer-fusion of the central slab to the photonic crystal. In well-fabricated samples, the polariton lifetime in our 3D PBG microcavities can be much longer than 130 ps, while efficient phonon scattering facilitates equilibration of the polariton gas in $\lesssim 1$ ps[11].

EFFECT OF EXCITON INHOMOGENEOUS AND HOMOGENEOUS BROADENING

As a result of polariton motional narrowing, inhomogeneous broadening within a given monolayer has only a minor effect on BEC[18–20]. Inhomogeneous broadening between different monolayers is modeled by a Gaussian random shift of the exciton emission energy in each monolayer, $E_{X0} \to E_{X0} + \delta E_l$, $l = 1, 2, 3$. The root mean square deviation of the vacuum Rabi splitting and the polariton dispersion depth V_{lp}, calculated as a function of exciton inhomogeneous broadening δE_{X0}, are shown in Fig. 6. The results for the three types of cavity are almost the same. The fluctuation of the vacuum Rabi splitting is considerably smaller than the exciton inhomogeneous broadening due to averaging among different monolayers[14], whereas the fluctuation of the dispersion depth V_{pl} is comparable to δE_{X0}. Nevertheless, for inhomogeneous broadening less than 10 meV, the dispersion depth remains larger than 48 meV enabling BEC up to 500 K (370 K) for the SP (woodpile) PC cavity.

Exciton homogeneous broadening is considerable in $MoSe_2$ at room temperature due to phonon scattering[11]. Optical measurements reveal a broadening of 50 meV in Ref. [5].

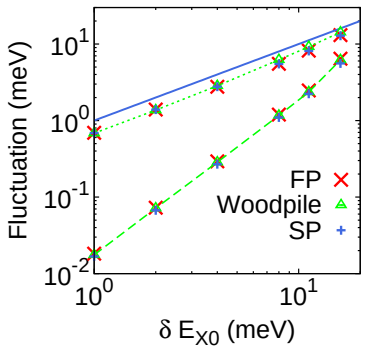

FIG. 6. Supplementary Figure S2. Root mean square deviation of the vacuum Rabi splitting (points linked by dotted curve) and the dispersion depth of polariton V_{lp} (points linked by dashed curve) as functions of the root mean square deviation of the exciton emission energy δE_{X0} when the detuning is $\Delta = 0$. The solid reference line denotes fluctuation equal to the exciton inhomogeneous broadening δE_{X0}.

Picosecond phonon scattering[11] facilitates thermal equilibration of polaritons within several picoseconds. Homogeneous broadening slightly degrades the vacuum Rabi splitting and the polariton dispersion depth. If the homogeneous broadening is described by a imaginary part of exciton energy, $i\Gamma$, the vacuum Rabi splitting is reduced from $2\hbar\Omega = 80$ meV to $2\sqrt{\hbar^2\Omega^2 - \Gamma^2/4} = 62$ meV at zero detuning for $\Gamma = 50$ meV. For a detuning of $\Delta = 40$ meV, exciton homogeneous broadening of $\Gamma = 50$ meV reduces the lower-polariton dispersion depth V_{lp} by 5.5 meV. The highest transition temperature is then reduced from 590 K to 560 K. If an inhomogeneous broadening of 30 meV is taken into account as well, the transition temperature will be reduced to 430 K which is still above room-temperature. This suggests that polaritons in woodpile and SP PC microcavities are robust against electronic and photonic disorder and exciton homogeneous broadening, enabling above room-temperature polariton BEC in realistic systems.

[1] Xiao D., Liu, G.-B., Feng, W., Xu, X. & Yao, W. Coupled spin and valley physics in monolayers of MoS_2 and other group-VI dichalcogenides. *Phys. Rev. Lett.* **108**, 196802 (2012).

[2] Ross, J. S. *et al.* Electrical control of neutral and charged excitons in a monolayer semiconductor. *Nat. Commun.* **4**, 1474 (2013).

[3] Haug, H. & Koch, S. W. *Quantum theory of the optical and electronic properties of semiconductors*, Chap. 10, (World Scientific, 2009).

[4] Ramasubramaniam, A. Large excitonic effects in monolayers of molybdenum and tungsten dichalcogenides. *Phys. Rev. B* **86**, 115409 (2012).

[5] Ugeda, M. M. *et al.* Observation of giant bandgap renormalization and excitonic effects in a monolayer transition metal dichalcogenide semiconductor. arXiv:1404.2331, Nat. Mater. in press.

[6] Kumar, N., He, J., He, D., Wang, Y. & Zhao, H. Valley and spin dynamics in $MoSe_2$ two-dimensional crystals. *Nanoscale*, **6**, 12690 (2014).

[7] Kumar, N. *et al.* Exciton-exciton annihilation in $MoSe_2$ monolayers. *Phys. Rev. B* **89**, 125427 (2014).

[8] Mermin, N. D. & Wagner, H. Absence of ferromagnetism or antiferromagnetism in one- or two-dimensional isotropic Heisenberg models. *Phys. Rev. Lett.* **17**, 1133-1136 (1966).

[9] Bhattacharya, P. *et al.* Room temperature electrically injected polariton laser. *Phys. Rev. Lett.* **112**, 236802 (2014).

[10] Horzum, S. *et al.* Phonon softening and direct to indirect band gap crossover in strained single-layer $MoSe_2$. *Phys. Rev. B* **87**, 125415 (2013).

[11] Jin, Z., Li, X., Mullen, J. T. & Kim, K. W. Intrinsic transport properties of electrons and holes in monolayer transition-metal dichalcogenides. *Phys. Rev. B* **90**, 045422 (2014).

[12] Ogawa, S., Imada, M., Yoshimoto, S., Okano, M. & Noda, S. Control of light emission by 3D photonic crystals. *Science* **305**, 227-229 (2004)

[13] Noda, S., Fujita, M., & Asano, T. Spontaneous-emission control by photonic crystals and nanocavities. *Nature Photon.* **1**, 449-458 (2007).

[14] Jiang, J. H. & John, S. Photonic crystal architecture for room temperature equilibrium Bose-Einstein condensation of exciton-polaritons. *Phys. Rev. X* **4**, 031025 (2014).

[15] Chamlagain, B. *et al. ACS Nano* **8**, 5079-5088 (2014)

[16] Wang, X. *et al.* Chemical vapor deposition growth of crystalline monolayer $MoSe_2$. *ACS Nano* **8**, 5125-5131 (2014).

[17] Shim, G. W. *et al.* Large-area single-layer $MoSe_2$ and its van der Waals heterostructures. *ACS Nano* **8**, 6655-6662 (2014).

[18] John, S. & Yang, S. Electromagnetically induced exciton mobility in a photonic band gap.

Phys. Rev. Lett. **99**, 046801 (2007).

[19] Yang, S. & John, S. Exciton dressing and capture by a photonic band edge. *Phys. Rev. B* **75**, 235332 (2007).

[20] Kavokin, A. V. & Malpuech, G. *Cavity polaritons* (Elsevier, Amsterdam, 2003), chap. 3.